Comprehensive characterization of Gunn oscillations in $In_{0.53}Ga_{0.47}As$ planar diodes

Y Lechaux[1,5] (iD), I Íñiguez-de-la-Torre[2], J A Novoa-López[2], Ó García-Pérez[3], H Sánchez-Martín[2], J F Millithaler[4], D Vaquero[1], J A Delgado-Notario[1] (iD), V Clericò[1], T González[2] and J Mateos[2,5] (iD)

[1] Laboratory of Nanoelectronics and Nanomaterials, University of Salamanca, Salamanca, Spain
[2] Department of Applied Physics, University of Salamanca, Salamanca, Spain
[3] Yebes Observatory, Instituto Geográfico Nacional, Yebes, Spain
[4] Department of Electrical and Computer Engineering, University of Massachusetts Lowell, Lowell, MA, United States of America

E-mail: yoann.lechaux@usal.es and javierm@usal.es

CrossMark

Abstract

In this work, $In_{0.53}Ga_{0.47}As$ planar Gunn diodes specifically designed for providing oscillations at frequencies below 30 GHz have been fabricated and characterized. Different types of measurements were used to define a set of consistent methods for the characterization of the oscillations that can be extended to the sub-THz frequency range. First, negative differential resistance and a current drop are found in the *I–V* curve, indicating the potential presence of Gunn oscillations (GOs), which is then confirmed by means of a vector network analyzer, used to measure both the S_{11} parameter and the noise power density. The onset of unstable GOs at applied voltages where the negative differential resistance is hardly visible in the *I–V* curve is evidenced by the observation of a noise bump at very low frequency for the same applied voltage range. Subsequently, the formation of stable oscillations with an almost constant frequency of 8.8 GHz is observed for voltages beyond the current drop. These results have been corroborated by measurements performed with a spectrum analyzer, which are fully consistent with the findings achieved by the other techniques, all of them applicable to Gunn diodes oscillating at much higher frequencies, even above 300 GHz.

Keywords: Gunn oscillations, III-V semiconductors, InGaAs, nanofabrication, RF measurements, noise power density

1. Introduction

High frequency technologies in the RF (sub-THz) and THz ranges are of high interest due to their broad field of applications, from high-speed communications to medical imaging [1, 2]. Different types of THz sources have been developed, such as thermal sources based on a mercury lamp, lasers sources like quantum cascade lasers or other solid-state electronic sources [3]. The most common solid-state THz and

sub-THz sources are based on the frequency multiplication of lower frequency fundamental oscillations generated by Gunn diodes. Gunn diodes, also called transferred electron devices, were discovered in 1963 by J.B. Gunn using GaAs as base material [4, 5]. The frequency of oscillations of Gunn diodes is determined by the anode-cathode distance (L_{AC}), which in typical vertical devices corresponds to the thickness of the epitaxial layer. As an alternative, planar structures are being explored, since they offer important advantages such as a simpler technological process (without the need of air bridges) and design flexibility (the oscillation frequency is not fixed by the epitaxial layer so that devices generating different frequencies

can be fabricated on the same wafer) [6]. In this case, the anode and cathode contacts are placed on the same active layer, and the reduction of the spacing between the two contacts can be used to increase the frequency of oscillations. Finally, the planar geometry of Gunn diodes facilitates their free space coupling by means of the integration with THz antennae [6]. Different III–V materials have been used to fabricate planar Gunn diodes, such as GaAs [6, 7], InP [8] or InGaAs [9–11]. For example, planar Gunn diodes based on AlGaAs/GaAs heterojunctions showed oscillations at 108 GHz [6] and the use of AlGaAs/In$_{0.23}$Ga$_{0.77}$As channels increases that frequency to 118 GHz [12]. The use of doped In$_{0.53}$Ga$_{0.47}$As Gunn layers allowed to take a leap forward, since diodes fabricated with 1.3 μm and 600 nm anode-cathode spacing were shown to exhibit oscillations at frequencies of about 164 GHz [10] and 307 GHz [11], respectively. Moreover the planar geometry provides the advantage that a contact shaping can be used to improve the efficiency of the Gunn oscillations (GOs) [13] or even generating components at frequencies above the fundamental transit time harmonic [14].

InAlAs/In$_{0.53}$Ga$_{0.47}$As heterojunctions could also be of interest, hopefully providing ultra-fast Gunn-like oscillations above THz frequencies, as predicted by Monte Carlo simulations [15]. New devices called self-switching diodes have been proposed as promising candidates to exhibit high-frequency GOs in the sub-THz range [16, 17]. Focusing the electric field by shaping the profile of nanochannels, they should be able to improve the efficiency of planar Gunn diodes and even help to achieve the challenging fabrication of GaN Gunn diodes [18–21].

In spite of these efforts, nowadays, the development of compact room temperature, tunable and low-cost powerful THz sources is still a challenge. From our experience in fabricating and characterizing sub-THz devices [22–25], we have learnt that once a given device potentially exhibiting high frequency oscillations has been fabricated, it is very difficult to experimentally confirm their presence. In some cases, the AC power generated is too small, in others the oscillations take place at too high frequencies, so that their detection becomes difficult. Several complementary techniques can be used to this end, namely measurements of: i) the DC I–V curve [26], ii) the S_{11} parameter (reflection coefficient) [27–29], iii) the power spectrum [6, 10, 11] or iv) even the noise at frequencies lower than that of the oscillation [30–33]. These techniques should provide coherent results when used to identify GOs in a given device. In this regard, recent advances in the state-of-the-art of RF measurement equipment have emerged, providing with new functionalities that allow to improve the characterization of high frequency devices with unprecedented levels of precision and speed. In this work, we report on the fabrication of In$_{0.53}$Ga$_{0.47}$As planar Gunn diodes specifically designed for providing GOs at frequencies below 30 GHz, with the objective of evidencing their presence and precisely characterizing them by all these techniques, thus checking their consistency, correlation, pros and cons, and also possible discrepancies among them. We remark that the attained conclusions can in principle be readily extended to diodes oscillating at much higher frequencies in the sub-THz range.

We initially present the fabrication process of the In$_{0.53}$Ga$_{0.47}$As planar Gunn diodes that are then used as test structures to evaluate the capabilities of several on-wafer electrical (DC and RF) characterization techniques. We put emphasis on achieving consistent results when performing different measurements on the same device. In a first part, the study is performed using a vector network analyzer (VNA) to precisely measure both the S_{11} parameter and the noise power generated by the diodes. In a second part, we employ a real-time spectrum analyzer (RSA) to measure the power spectrum of the generated signal. The results obtained by the different techniques are finally compared and the pros and cons of each of them are discussed.

2. Experimental details

2.1. Fabrication

In$_{0.53}$Ga$_{0.47}$As planar Gunn diodes have been fabricated in the cleanroom of the University of Salamanca using In$_{0.53}$Ga$_{0.47}$As doped active layers lattice-matched grown on InP. The epitaxial layer follows the design used by the group at the University of Glasgow [10]. It consists of a 100 nm layer doped at 8×10^{16} cm^{-3} on top of a buffer made of In$_{0.52}$Al$_{0.48}$As grown on an InP substrate (100), followed by a 50 nm cap layer doped at 2×10^{18} cm^{-3}. The technological process starts with the definition of a mesa of 14 μm $\times$ 14 μm using deep UV (284 nm) lithography. The etching of the different layers is performed with a DC bias controlled ICP-RIE dry etching process using a Cl$_2$/BCl$_3$ gas mixture. Then, Ti/Au ohmic contacts were deposited at low pressure (10^8 mbar) using e-beam evaporation, showing a specific contact resistivity ρ_C of about 1×10^{-5} Ω cm^{-2}. In order to avoid as much as possible RF losses, coplanar waveguide (CPW) accesses were also defined in the same process with a 30 μm signal line and 5 μm spacing in ground-signal-ground (GSG) configuration, compatible with our 100 μm pitch RF probes and providing a characteristic impedance of about 32 Ω. Such low impedance CPW was intended for the fabrication of high power Gunn diodes (with much larger widths), but in this case we used a small mesa in order to decrease the heating-related problems, so that, on the one hand, the characterization process is simpler, and, on the other, it allows for increasing the applied bias range. The distance L_{AC} between the two contacts, anode and cathode, is about 12 μm, see figure 1(a). This relatively long L_{AC} was also purposely chosen in order to ensure that the frequency of the generated GOs is not too high, so that they can be reliably measured with the available equipment. Assuming the electron saturation velocity to be about 10^5 m s^{-1}, the oscillation frequency of the diodes, once stable, is expected to be around 8.3 GHz.

2.2. Electrical characterization setup

The DC characterization was performed with a Keithley 4200-SCS semiconductor analyzer. RF measurements were carried out with: (i) an Agilent PNA X 5244 VNA with Option 029 (noise measurement capability) in order to extract the
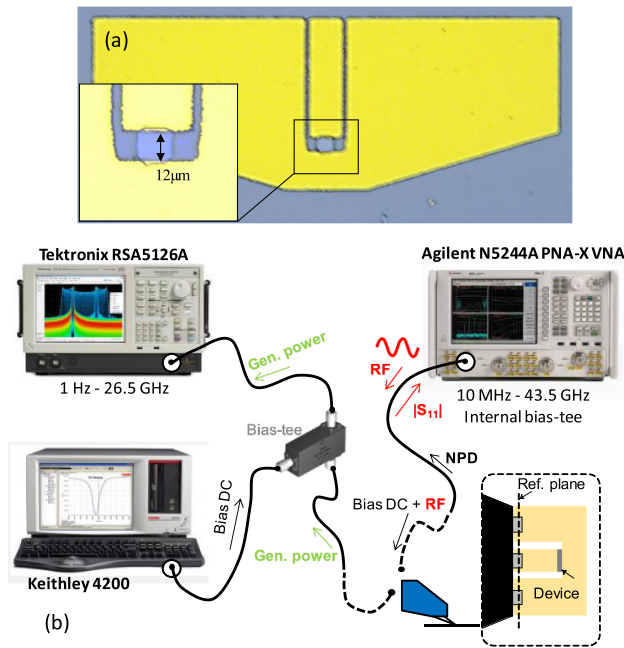
Figure 1. (a) Optical microscope image of the $In_{0.53}Ga_{0.47}As$ planar Gunn diode with a zoom on the active part (inset) and (b) setup of the RF measurements using the vector network analyzer (VNA) or the spectrum analyzer (RSA), and the semiconductor analyzer to bias the devices through the bias-tee (internal in the VNA and external in the case of the measurements with the RSA). Allstron coplanar waveguide probes with GSG configuration and 100 μm pitch were used.

$|S_{11}|$ parameter and the noise power density (NPD), and (ii) a Tektronix RSA5126A RSA to obtain the generated power. The VNA covers the frequency range between 10 MHz and 43.5 GHz, and the RSA between 1 Hz and 26.5 GHz. The setup for RF characterization is shown in figure 1(b). A bias tee, internal in the case of the VNA, is used to apply different bias voltages V_{DC}. All measurements were performed at room temperature.

3. Characterization

3.1. DC measurements

Figure 2 shows the current-voltage (*I–V*) characteristic measured in the $In_{0.53}Ga_{0.47}As$ planar Gunn diode at room temperature.

Three different regimes are observed:

(a) Between $V_{DC} = 0$ V and 4 V, the current increases with the voltage, first linearly and then starts saturating, as in a typical semiconductor resistor.

(b) Between $V_{DC} = 4$ V and around $V_{DC} = 6.5$ V, the current saturates or even slightly decreases and then a sharp drop takes place. Both the slight decrease and the drop of the current are indicators of the negative differential resistance (NDR) potentially caused by the onset of GOs [26]. However, other possible explanations could be given, like self-heating for the slight NDR, or trap activation for the
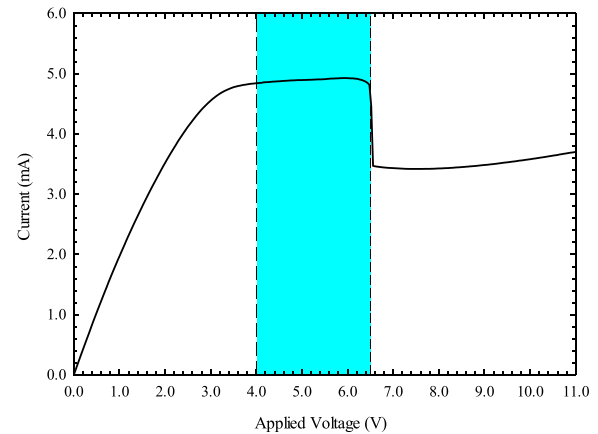

Figure 2. Current-voltage characteristic of the $In_{0.53}Ga_{0.47}As$ Gunn diode with L_{AC} of 12 μm.

current drop. The presence of GOs can only be confirmed by means of RF measurements, as we will do in the following. At this point, we should also make clear that the current drop does not always happen at the same voltage for a given device; in consecutive sweeps its position may shift by roughly ±0.5 V.

(c) Above around $V_{DC} = 7$ V the current increases with the voltage, sometimes showing some bumps at random positions.

3.2. VNA measurements

3.2.1. S-parameter. In order to confirm the presence of oscillations, as first indicator we realized standard VNA S-parameter measurements. An on-wafer Short-Open-Load-Thru calibration was first made in order to remove the losses and locate the reference plane for the RF measurements at the tip of the CPW probe. Such diode 1-port configuration allows measuring only the reflected power, so S_{11} can be obtained. The values obtained for $|S_{11}|$ are shown in figure 3(a) for a frequency range between 100 MHz and 40 GHz and bias voltages from 0 V to 11 V. To help identifying the position in frequency of the different features observed in $|S_{11}|$, an offset of +1 was added to the values in each curve with respect to the previous one (except for $V_{DC} = 0$ V). At equilibrium $|S_{11}(f)| \simeq 0.83$, being consistent with the resistance of about 500 Ω exhibited by the diode *I–V* curve of figure 2. It can be observed that for bias below $V_{DC} = 4$ V, an increase of $|S_{11}|$ with voltage takes place due to the higher resistance of the device and increased mismatch with the 50 Ω impedance of the VNA. In this bias range, the values of $|S_{11}|$ are below unity in the complete measured frequency range, as expected for a passive device. For applied voltages between $V_{DC} = 5$ V and 6 V, the values of $|S_{11}|$ are above unity and show a resonance with a relatively broad peak (going from positive to negative values) at frequencies higher than 20 GHz (and eventually at its harmonics), indicating the onset of the oscillation regime [27, 28]. Finally, for $V_{DC} > 7$ V, the resonance-like peaks become very narrow (at a fundamental frequency and its harmonics), which is an

indication of stable GOs. We found that the fundamental frequency of the oscillations, f_{GO}, decreases with increasing bias voltage, being at about 9.4 GHz for $V_{DC} = 7$ V and decreasing to 8.8 GHz at $V_{DC} = 11$ V. Using the expression $v = L_{AC} \cdot f_{GO}$ as a first estimation of the Gunn domain velocity v, which neglects the presence of a dead zone, we found a value of about 1.1×10^5 m s^{-1} for $f_{GO} = 8.8$ GHz, which is within the theoretical range expected for the saturation velocity of In$_{0.53}$Ga$_{0.47}$As ($\sim 10^5$ m s^{-1}) [34].

Thus, from the information provided by $|S_{11}|$, we can conclude that the device seems to exhibit GOs, whose frequency can be identified by abrupt resonance-like changes in $|S_{11}|$ beyond a threshold voltage V_{TH1} of about 4 V, which is consistent with the saturation/NDR observed in the *I–V* characteristic. We could also define a second threshold voltage, V_{TH2}, of about 6–7 V, for the onset of stable GOs.

3.2.2. Noise power density. Previous works have predicted and evidenced experimentally an anomalous increase of the noise at lower frequencies at the onset of higher-frequency Gunn or other type of oscillations [30–33], which then vanishes once the oscillations are stable. This effect can be used as an indicator to anticipate the presence of very-high-frequency GOs in cases in which the lack of adequate equipment or low-power levels makes difficult a proper direct detection. As a second indicator of the onset and presence of stable oscillations in our diode, we have measured the NPD in the current by means of the same VNA used in the previous section, which is equipped with an ultra-sensitive receiver for source-corrected noise figure measurements (option 029). This noise-measuring capability of the VNA is a recent add-on to this type of equipment which is highly valuable for our purpose of precisely measure the absolute power generated by the Gunn diodes, which, in addition, is made simultaneously to the standard S-parameter measurements. The noise measurement requires a specific calibration using a noise source with hot and cold states, which allows for removing the effect of the noise and losses of the cables, thus improving the accuracy of the detected power and sensitivity of the instrument as compared with a conventional spectrum analyzer [33].

The VNA provides two kind of NPD measurements [35]: (i) the power directly delivered/injected to the receiver in a given bandwidth (DUTNPDI), where any mismatch between the receiver and the DUT (Device Under Test) is ignored, and (ii) the available noise power (DUTNPD), computed by removing the effect of the impedance mismatch of the diode in the reference plane by means of the $|S_{11}|$ value, which is measured almost simultaneously. The VNA alternates automatically, in a fast sweep, between *S*-parameters and high-accuracy noise figure measurements. Basically, the DUTNPD is the maximum power available from the DUT when the impedance of the noise port is equal to the output match of the DUT. At zero-bias, the spectral response is flat and DUTNPD = $10 \cdot \log(k_B T_0)$, k_B being the Boltzmann constant, thus taking the well-known value of -174 dBm Hz^{-1} at room temperature ($T_0 = 290$ K) [33]. On the other hand, DUTNPDI = $10 \cdot \log[k_B T_0 \cdot (1-|S_{11}|^2)]$, which in our case takes the value
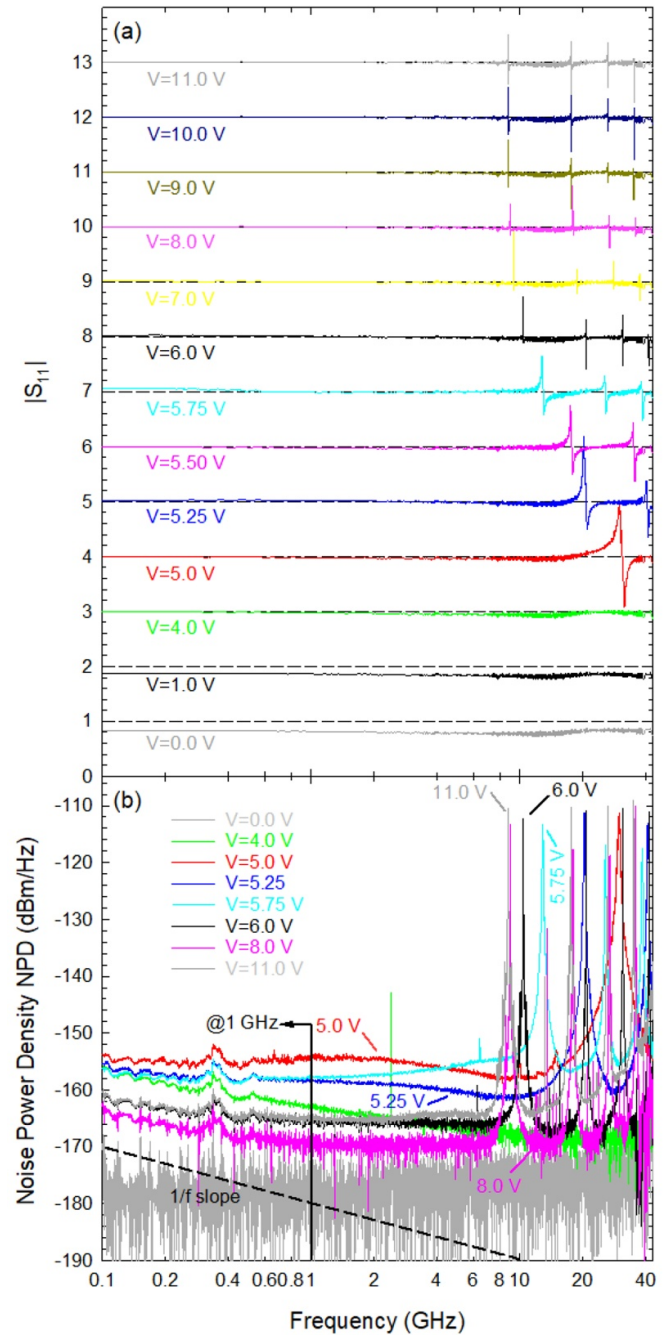

Figure 3. (a) VNA measurements for different voltages in the In$_{0.53}$Ga$_{0.47}$As Gunn diode with $L_{AC} = 12$ μm in a frequency range between 100 MHz and 43.5 GHz: $|S_{11}|$ parameter. For clarity, a +1.0 offset has been added to each curve with respect to the previous one, with no offset for 0 V. Dashed lines indicate the level of $|S_{11}| = 1$ for each bias. (b) Noise power density at the VNA receiver (DUTNPDI). Undesired radiofrequency interferences appear at around 350 MHz and 2.4 GHz, which correspond to the well-localized communication services of radio and Wi-Fi, respectively.

of -179 dBm Hz^{-1}. Even if DUTNPD is the quantity typically used to present noise measurements, we have decided to show here only the value of DUTNPDI, called from now on NPD, for two reasons: (a) the calculation of the power mismatch through $|S_{11}|$ becomes uncertain in the presence of
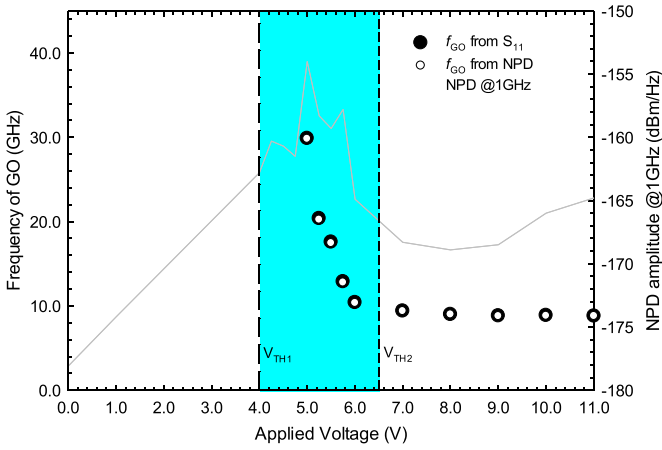
Figure 4. Frequency of the GOs (left axis) as extracted from the peaks obtained in the measurements made with the VNA, both of $|S_{11}|$ (figure 3(a), black circles), and of NPD (figure 3(b), white circles). Also plotted is the NPD at 1 GHz (right axis, shaded area). The unstable GO region between V_{TH1} and V_{TH2} is also indicated.

GOs ($|S_{11}| > 1$), and (b) its value can be better and fair compared with the measurements made in a similar way with the RSA, where no mismatch is taken into account, as we will explain in next section.

The incident NPD measured by the VNA receiver as a function of frequency for different bias voltages is shown in figure 3(b). As mentioned before, when zero-bias voltage is applied, the spectral response is lower than -174 dBm Hz^{-1} (due to the impedance mismatch, about -5 dB at low frequency, given by the 500 Ω resistance of the Gunn diode). Then, when increasing the applied voltage, the NPD increases and $1/f$ and hot carrier noise arises. Interestingly, in the range of unstable GOs, for biases between V_{TH1} and V_{TH2}, two phenomena are observed. First, broad peaks are found at high frequency ($f > 20$ GHz), indicating the incoherent generation of oscillations given by the chaotic formation of Gunn domains at different distances from the cathode. In addition, as in [33], a broad frequency hump is observed at low frequency (around 1 GHz), which is also linked to this chaotic distribution of transit times, indicating that unstable GOs are not taking place at a fixed frequency; on the contrary, its frequency fluctuates around its central value. The NPD at 1 GHz and the frequency of the fundamental peak (f_{GO}) are shown in figure 4 as a function of the applied voltage, jointly with the frequency of the fundamental peak in $|S_{11}|$. As observed, the noise at 1 GHz increases during the onset of the oscillations. For voltages up to V_{TH2}, both the amplitude of the noise hump and the frequency of the GOs, f_{GO}, decrease, and the peak gets narrower; see figure 3(b). For $V_{DC} > V_{TH2}$, the noise hump completely disappears, f_{GO} takes a steady value of about 8 GHz, and its width is very narrow, indicating that the regime of stable GOs has been reached. This limit approximately coincides with the sharp current drop in the *I–V* curve. It is also important to remark that, as shown in figure 4, the frequencies of the fundamental peaks observed in the measurements of $|S_{11}|$ and NPD perfectly agree, showing that both measurements can be used for characterizing the frequency of the GOs.

3.3. RSA measurements

As last characterization technique, we have used the RSA to measure the power generated by the diode as a free-running oscillator, just applying a DC bias. The generated power P_{dBm} was measured using the Tektronix RSA5126A, in figure 1, and then it was normalized according to the resolution bandwidth RBW as $P_{dBm/Hz} = P_{dBm} - 10 \cdot \log(RBW)$.

Figures 5(a) and (b) show the measured generated power $P_{dBm/Hz}$ as a function of frequency in the two ranges of unstable and stable GO, for $V_{DC} = 5.8$ V and 10 V, respectively. The real-time capability of the spectrum analyzer is able to fast perform multiple measurements of the power at each frequency sweep and present not only the peak or average values, but also a histogram-like color map display with all measured values (red showing the most probable values and dark blue the less probable ones) [36]. The peak and average detected power are plotted in figures 5(a) and (b) with pink and cyan solid lines, respectively. We have to remark that it is not possible to make a direct comparison between the measurements of the power made with the VNA and the RSA. First, because the values of the output power provided by the RSA are artificially increased by the noise factor of its internal receiver, NFRSA, which imposes a positive offset on the displayed spectrum. Knowing that the displayed average noise level (DANL) of the RSA is 155 dBm Hz^{-1} (typical below 4 GHz), corresponding to the noise floor of our instrument without using the internal preamplifier [37], we can estimate this offset as NFRSA = DANL + 174 dBm Hz^{-1} to be around 21 dB [37]. In addition, the losses of the cables have not been taken into account, since in this case no previous calibration process has been made.

As observed, disregarding the absolute power level obtained with the RSA, the results of the measurements are quite similar to those obtained with the VNA. For $V_{DC} = 5.8$ V, a broad frequency peak at around 8.95 GHz is obtained, with a full width at tenth maximum (FWTM, calculated as the width of the distribution at a level 10 dB below the peak of the average trace) of about 20 MHz. In this case, the GOs are still unstable. At $V_{DC} = 10$ V, the peak of the generated power shifts to a lower frequency of 7.13 GHz and it is much narrower (FWTM of about 2 MHz), meaning the GOs are now stable.

Moreover, the power spectra generated by the diode, represented in figure 5(c) in a wider frequency range (between 100 MHz and 20 GHz) and for applied voltages from 0 V to 8 V, shows identical features to those of the NPD measured with the VNA [figure 3(b)]. In order to better detect the low power features of the spectrum, we have plotted here the traces obtained with the peak detector configuration of the RSA [pink lines of figures 5(a) and (b)]. This makes that the values of the RSA detected power are slightly higher than those of the NPD, even when considering that the NFRSA imposes a uniform positive offset of about 20 dB.

Going into details, as in the case of the VNA measurements, broad peaks at high frequency (above 10 GHz) are observed for applied voltages between V_{TH1} and V_{TH2}, in coincidence with the low-frequency hump around 1 GHz. Figure 6 shows
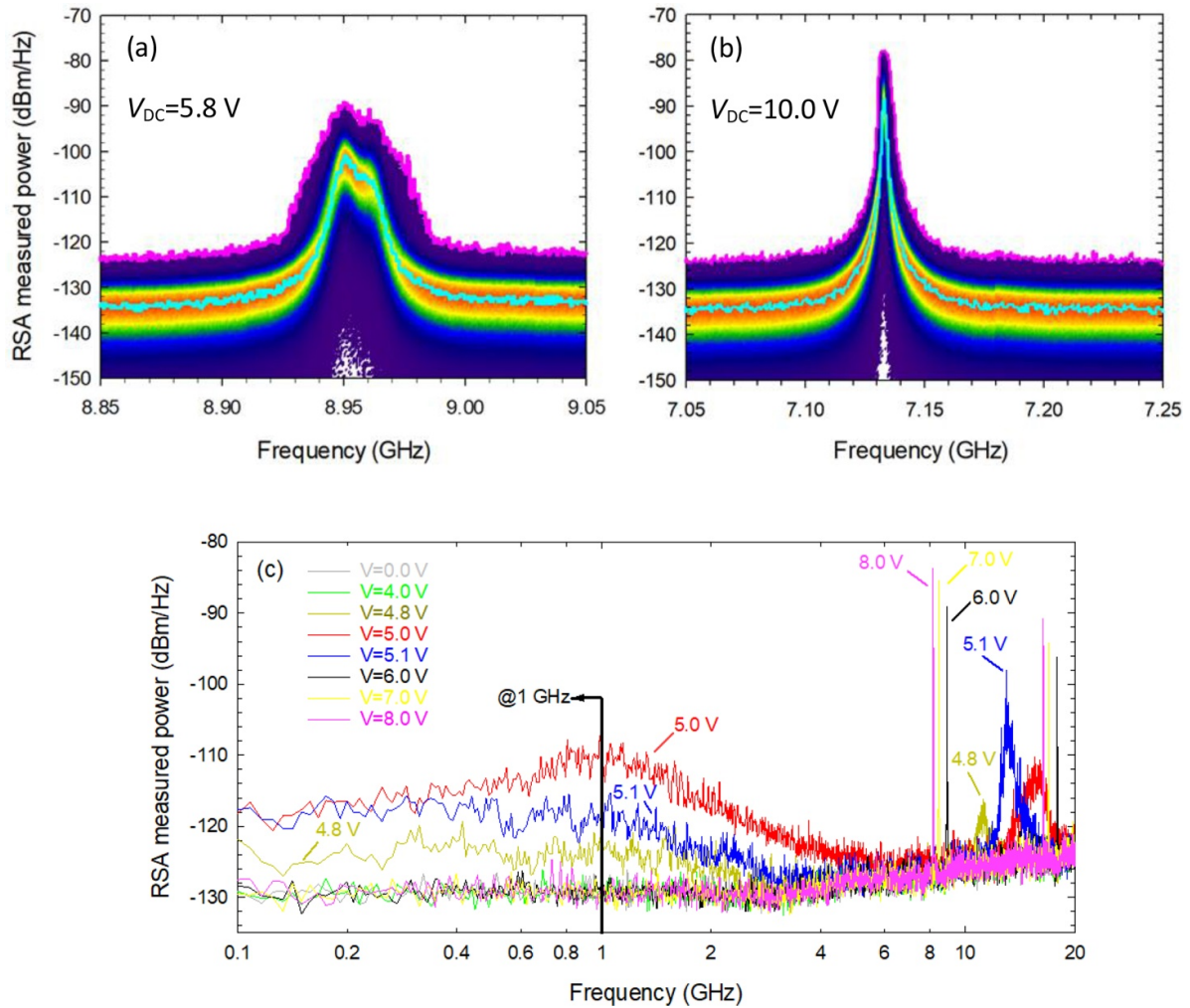
Figure 5. RSA measurements of the power generated by the diode with $L_{AC} = 12\ \mu$m using the DPX®spectrum display for representing the time domain measurements of the power spectrum in a colour map, where different frequency-of-occurrence values are displayed in different colours (red for highly probable values, dark blue for less frequent ones), for two applied voltages: (a) 5.8 V, showing unstable GOs, and (b) 10 V, showing stable GOs. Peak and average values are shown with pink and cyan solid lines, respectively. (c) Peak power spectra for different bias points. $RBW = 100$ kHz in all cases.

how, also in the RSA, the presence of the hump (shaded area) at 1 GHz perfectly agrees with a strong decrease of the f_{GO} with the increase of the applied voltage, thus confirming that unstable GOs appear between V_{TH1} and V_{TH2}. Remarkably, the hump is better observed in the RSA measurements than in the VNA ones due to the real-time detection of the spectrum, that allows plotting the peak power observed at each frequency, so that the noise is better revealed, even if the displayed power level is not the real one. Another advantage of the measurement performed using the RSA is the manual control not only of the *RBW*, but also of the acquisition bandwidth, that allows for the detection of random or slowly varying events, as it is the case of the unstable GOs. As such, the RSA is especially appropriate for a qualitative characterization of the appearance of the GOs, while the well-calibrated NPD values from the VNA can be taken as the accurate power generated by the Gunn diodes.

Figure 6 compares the bias dependence of the f_{GO} as measured with the RSA and the VNA. Even if their behavior is similar, some discrepancies are observed, both in the bias range for unstable GOs (which is shifted to lower voltages in the RSA measurements) and in the frequency of the stable GOs (slightly lower in the RSA measurements). During the intense characterization process, which reveals the robustness of the device, we have observed that even if the qualitative behavior of the Gunn diodes stays the same, there has been a variant response as more measurements were carried out. The VNA and RSA measurements were not done at the same time, what explains the dissimilarities observed in figure 6. Finally, we want to remark that this dispersion in the results comes also from the fact that the Gunn diodes are not connected to any resonant circuit, which is typically used in practical applications in order to fix the oscillation frequency.
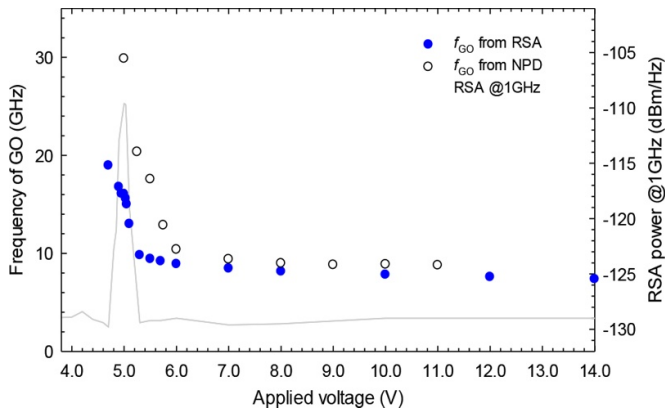
Figure 6. Comparison of the frequency of the GOs (left axis) as a function of bias extracted with the RSA (blue circles) and with the VNA (white circles, values from figure 4). The shaded area corresponds to the value of the power measured with the RSA @1 GHz, confirming that the low frequency hump evidences the bias region where unstable GOs take place.

4. Conclusion

In$_{0.53}$Ga$_{0.47}$As planar Gunn diodes with a length of 12 μm have been fabricated and characterized in DC and RF. A comprehensive analysis of the GOs present in the device has been performed by combining different measurement techniques, which provide consistent results. The DC measurements showed a clear current drop, indicating that GOs might be present in the device. The RF characterizations confirmed that evidence. First, using a VNA, a clear NDR is identified in the *S* parameter measurements, $|S_{11}| > 1$, beyond a first threshold voltage V_{TH1}. Stable GOs have been identified beyond a second threshold voltage $V_{TH2} > V_{TH1}$ by a resonance in the value of S_{11} at a frequency of about 8.8 GHz (measured with the VNA at 11 V), value which agrees well with the electron saturation velocity of In$_{0.53}$Ga$_{0.47}$As. Besides, an increase of the noise in a broad frequency range around 1 GHz has been observed for voltages at the onset of the oscillations, associated with unstable and randomly distributed Gunn domains formation, a precursor of the presence of stable oscillations at higher biases. These observations were confirmed measuring the generated power using a RSA. In spite of the slight shift in the threshold voltage and the frequency of the GOs, the increase of the power measured at around 1 GHz was also observed. A remarkable consistency between the results of the different characterization techniques we have used was found, the real-time capability of the RSA being very useful to enhance the detection of the onset of the GOs and the low frequency hump, while the precisely calibrated and highly-accurate NPD measurements made with the VNA allow for the absolute power measurement of the GO mechanism. As a conclusion, for the measurement of the power generated by the Gunn diodes, as compared with the VNA, the use of a RSA offers much more control and flexibility in terms of their RBW and acquisition bandwidths, but, on the other hand, losses are not calibrated and it lacks the functionality to measure the impedance of the DUT.

ORCID iDs

Y Lechaux ⑩ https://orcid.org/0000-0002-9799-0842
J A Delgado-Notario ⑩ https://orcid.org/0000-0001-9714-8180
J Mateos ⑩ https://orcid.org/0000-0003-4041-7145

References

[1] Beard M C, Turner G M and Schmuttenmaer C A 2002 Terahertz spectroscopy *J. Phys. Chem.* B **106** 7146–59
[2] Lee Y S 2009 *Principles of Terahertz Science and Technology* (Boston, MA: Springer)
[3] Lewis R A 2014 A review of terahertz sources *J. Phys. D: Appl. Phys* **47** 374001
[4] Gunn J B 1963 Microwave oscillations of current in III–V semiconductors *Solid State Commun.* **1** 88–91
[5] Hilsum C 1962 Transferred electron amplifiers and oscillators *Proc. IRE* **50** 185–9
[6] Khalid A, Pilgrim N J, Dunn G M, Holland M C, Stanley C R, Thayne I G and Cumming D R S 2007 A planar gunn diode operating above 100 GHz *IEEE Electron Device Lett.* **28** 849–51
[7] Sekido K, Takeuchi T, Hasegawa F and Kikuchi S 1969 CW oscillations in GaAs planar-type bulk diodes *Proc. IEEE* **57** 815–6
[8] Eisele H and Kamoua R 2004 Submillimeter-wave inp gunn devices *IEEE Trans. Microwave Theory Tech.* **52** 2371–8
[9] Khalid A *et al* 2013 In$_{0.53}$Ga$_{0.47}$As planar gunn diodes operating at a fundamental frequency of 164 GHz *IEEE Electron Device Lett.* **34** 39–41
[10] Khalid A *et al* 2014 Terahertz oscillations in an In$_{0.53}$Ga$_{0.47}$As submicron planar gunn diode *J. Appl. Phys.* **115** 114502
[11] Maricar M I, Khalid A, Cumming D R S and Oxley C H 2016 Extraction of second harmonic from an InP based planar Gunn diode using diamond resonator for milli-metric wave frequencies *Solid State Electron.* **116** 104–6
[12] Li C, Khalid A, Caldwell S H P, Holland M C, Dunn G M, Thayne I G and Cumming D R S 2011 Design, fabrication and characterization of In0.23Ga0.77As-channel planar Gunn diodes for millimeter wave applications *Solid State Electron.* **64** 67–72
[13] Mindil A, Dunn G M, Khalid A and Oxley C H 2020 Investigation of contact edge effects in the channel of planar gunn diodes *IEEE Trans. Electron Devices* **67** 53–56
[14] Mindil A, Dunn G M, Khalid A and Oxley C H 2020 Investigation of high-frequency fine structure in the current output of shaped contact planar gunn diodes *IEEE Trans. Electron Devices* **67** 1946–51
[15] Pérez S, González T, Pardo D and Mateos J 2008 Terahertz Gunn-like oscillations in InGaAs/InAlAs planar diodes *J. Appl. Phys.* **103** 094516
[16] Song A M, Missous M, Omling P, Peaker A R, Samuelson L and Seifert W 2003 Unidirectional electron flow in a nanometer-scale semiconductor channel: A self-switching device *Appl. Phys. Lett.* **83** 1881–3

[17] Xu K Y, Wang G and Song A M 2008 Gunn oscillations in a self-switching nanodiode *Appl. Phys. Lett.* **93** 233506

[18] Sevik C and Bulutay C 2004 Gunn oscillations in GaN channels *Semicond. Sci. Technol.* **19** S188–90

[19] Íñiguez-de-la-torre A, Íñiguez-de-la-torre I, Mateos J, González T, Sangaré P, Faucher M, Grimbert B, Brandli V, Ducournau G and Gaquière C 2012 Searching for THz Gunn oscillations in GaN planar nanodiodes *J. Appl. Phys.* **111** 113705

[20] Millithaler J-F, Iñiguez-de-la-torre I, Iñiguez-de-la-torre A, González T, Sangaré P, Ducournau G, Gaquière C and Mateos J 2014 Optimized V-shape design of GaN nanodiodes for the generation of Gunn oscillations *Appl. Phys. Lett.* **104** 073509

[21] Vasallo B G, Millithaler J F, Íñiguez-de-la-torre I, González T, Ducournau G, Gaquière C and Mateos J 2014 Monte Carlo study of the operation of GaN planar nanodiodes as sub-THz emitters in resonant circuits *Semicond. Sci. Technol.* **29** 115032

[22] Torres J *et al* 2013 Nonlinear nanochannels for room temperature terahertz heterodyne detection *Semicond. Sci. Technol.* **28** 125024

[23] Iniguez-de-la-torre I *et al* 2014 Operation of GaN planar nanodiodes as THz detectors and mixers *IEEE Trans. Terahertz Sci. Technol.* **4** 670–7

[24] Westlund A *et al* 2015 Optimization and small-signal modeling of zero-bias InAs self-switching diode detectors *Solid State Electron.* **104** 79–85

[25] Daher C, Torres J, Iniguez-de-la-torre I, Nouvel P, Varani L, Sangare P, Ducournau G, Gaquiere C, Mateos J and Gonzalez T 2016 Room temperature direct and heterodyne detection of 0.28–0.69-THz waves based on GaN 2-DEG unipolar nanochannels *IEEE Trans. Electron Devices* **63** 353–9

[26] Ridley B K and Watkins T B 1961 Negative resistance and high electric field capture rates in semiconductors *J. Phys. Chem. Solids* **22** 155–8

[27] Li C 2012 Design and characterisation of millimetre wave planar Gunn diodes and integrated circuits *PhD Thesis* University of Glasgow

[28] Papageorgiou V, Khalid A, Li C, Steer M J and Cumming D R S 2014 Integration techniques of pHEMTs and planar Gunn diodes on GaAs substrates *Solid State Electron.* **102** 87–92

[29] Maricar M I, Khalid A, Dunn G, Greedy S, Thomas D, Cumming D R S and Oxley C H 2018 An electrical equivalent circuit to simulate the output power of an AlGaAs/GaAs planar gunn diode oscillator *Microw. Opt. Technol. Lett.* **60** 2144–8

[30] Kabashima S, Yamazaki H and Kawakubo T 1976 Critical fluctuation near threshold of gunn instability *J. Phys. Soc. Jpn.* **40** 921–4

[31] Shiktorov P, Starikov E, Gružinskis V, Varani L, Reggiani L, Macucci M and Basso G 2009 Giant enhancement of low-frequency noise as precursor for the onset of a high-frequency instability *AIP Conf. Proc.* **1129** 179

[32] Íñiguez-de-la-torre A, Íñiguez-de-la-torre I, Mateos J and González T 2011 Correlation between low-frequency current-noise enhancement and high-frequency oscillations in GaN-based planar nanodiodes: a Monte Carlo study *Appl. Phys. Lett.* **99** 062109

[33] García-Pérez Ó, Alimi Y, Song A, Íñiguez-de-la-torre I, Pérez S, Mateos J and González T 2014 Experimental assessment of anomalous low-frequency noise increase at the onset of Gunn oscillations in InGaAs planar diodes *Appl. Phys. Lett.* **105** 113502

[34] Karishy S, Ziadé P, Sabatini G, Marinchio H, Palermo C, Varani L, Mateos J and Gonzalez T 2016 Review of electron transport properties in bulk InGaAs and InAs at room temperature *Lith. J. Phys.* **55** 306–14

[35] Keysight noise figure application (available at: http://na. support.keys ight.com/pna/help/latest/Applications/Noise_ Figure.htm)

[36] Adnani A, Duplicy J and Philips L 2013 Spectrum analyzers today and tomorrow: part 1 towards filterbanks-enabled real-time spectrum analysis *IEEE Instrum. Meas. Mag.* **16** 6–11

[37] Tektronix RSA5126A datasheet (available at: https://www.tek.com/datasheet/spectrum-analyzers-datasheet)